

Probing QCD Phase Structure by Baryon Multiplicity Distribution

Atsushi Nakamura and Keitaro Nagata

RIISE, CMC, Hiroshima University, Higashi-Hiroshima 739-8527 Japan.

(Dated: May 6, 2013)

The canonical partition functions Z_n and the number distributions P_n which are observable in experiments, are related by a single parameter, the fugacities $\xi = \exp(\mu/T)$. With the charge parity invariance, Z_n and ξ can be determined. Thermodynamic quantities such as the number density susceptibility and the kurtosis are then calculated from the grand canonical partition function $Z(\xi, T) = \sum Z_n(T) \xi^n$, ($n = -N_{\max}, \dots, N_{\max}$), for any chemical potential μ , although the region over which the results are reliable for these quantities is constrained by N_{\max} . We then calculate the Lee–Yang zeros, which are the zeros of $Z(\xi)$ in the complex fugacity plane, as poles of $d \log Z(\xi)/d\xi$ by using the Cauchy integral theorem. With the help of a multiple precision library, this method provides any precision required without misidentification of the zeros.

We analyse Z_n from the net-proton number distributions recently measured at the Relativistic Heavy Ion Collider (RHIC) by assuming the net-proton number is approximately proportional to that of the baryon after the freeze-out, and calculate the moments. We also evaluate the Lee–Yang zero structures obtained from RHIC data and compare them with those obtained from lattice quantum chromodynamics (QCD) calculations.

Possible regions of QCD phase transition lines are estimated from the thermodynamics quantities and the Lee–Yang zeros. We discuss how the limited N_{\max} in both experimental and numerical studies affects the reliability of the thermodynamic results and Lee–Yang zeros.

When temperature and density are varied, QCD is expected to have a rich phase structure [1]. One of the most important challenges in particle and nuclear physics is to experimentally discover these phases that only appear under extreme conditions and to theoretically understand the nature of these phases. Such achievements would not only deepen our understanding of QCD but also extend our knowledge of the early universe and compact stars.

The Relativistic Heavy Ion Collider (RHIC) was built to explore properties of QCD matter [2], and has provided much valuable information [3, 4]. In addition, many phenomenological studies have also focused on the phases of QCD matter [5]. Although lattice QCD provides very precise information about QCD at finite temperatures [6], thirty years of numerical studies of lattice QCD at finite baryon number density are still far from yielding conclusive results because of a notorious sign problem [7, 8].

Recently net-proton multiplicity measurements at RHIC are gaining attention [9, 10] because they enable the QCD phase diagram to be explored [11]. In these measurements, the colliding energy is varied, and the trajectory (T, μ_B) in the QCD phase diagram may pass near the critical region. Even-by-event fluctuations are expected to encompass the critical point, where the correlation length changes. In particular, conserved quantities such as charge or baryon number may reveal possible correlations that existed inside the system before hadronization. (see Ref.[12] and references therein).

In this paper, we propose a method by which, even without experimental data near the phase transition, the observed number distribution data can be used to obtain more information about the QCD phase transition, and even without direct lattice QCD calculations at physical chemical potential regions, we can use the data to understand experimental multiplicity through the canonical

partition functions.

The grand partition function Z and the canonical partition function Z_n are related according to

$$Z(\xi, T) = \text{Tr} e^{-\beta(H - \mu \hat{N})} = \sum_{n=-N_{\max}}^{+N_{\max}} Z_n(T) \xi^n, \quad (1)$$

where $\xi = \exp(\mu/T)$. Here we assume that the number operator \hat{N} commutes with H , that is, \hat{N} is a conserved quantity. Because of the charge-parity symmetry, Z_n satisfies

$$Z_n = Z_{-n}. \quad (2)$$

The multiplicity distributions P_n observed in experiments are related to Z_n as

$$P_n(\xi) = Z_n \xi^n. \quad (3)$$

Using Eqs.(2) and (3), we can determine ξ and Z_n . Fig.1 shows the obtained ξ together with that by a freeze-out analysis in Ref.[13]. From the grand partition functions Eq.(1), the moments are evaluated using $\lambda_k(\xi) \equiv (\xi \frac{\partial}{\partial \xi})^k \log Z(\xi)$.

We assume that the net-proton multiplicity data are approximately proportional to those of the baryon. The proportionality factor has no effect on any of the results reported in this paper. This approximation is justified if (i) after the freeze-out, the net-proton number is effectively constant, or (ii) a created fireball is approximately iso-neutral.

The quantity N_{\max} in Eq.(1) is finite because of measurement statistics (simulation statistics and finite volume) in the experiments (lattice QCD). The finite nature of N_{\max} puts an upper bound on the chemical potential for which the calculation is valid. To estimate the effect

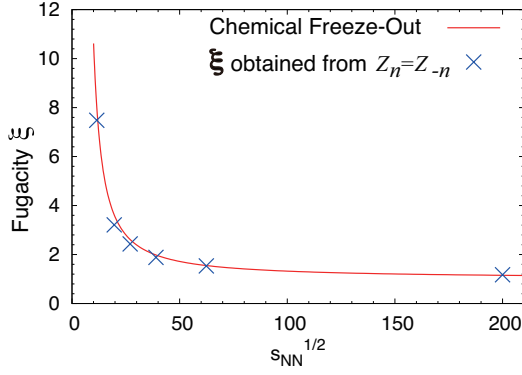


FIG. 1: Fugacity $\xi = \exp(\mu/T)$ as a function of the colliding energy \sqrt{s} . Plotted are those obtained from RHIC experiments (blue crosses) and the freeze-out results reported in Ref.[13].

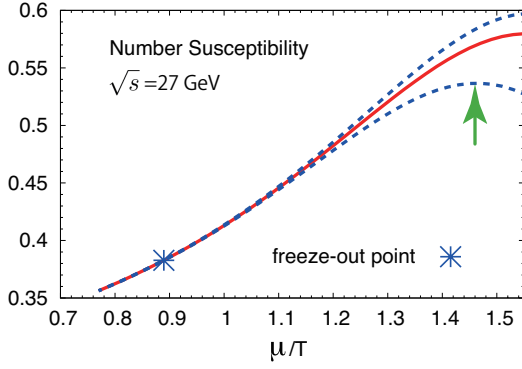


FIG. 2: The number susceptibility, λ_2/N_{\max} , at $\sqrt{s} = 27$ as a function of μ/T . The upper curve is obtained by raising the final three Z_n , ($n = N_{\max} - 2, N_{\max} - 1, N_{\max}$) by 15%. The lower curve results from dropping the final two Z_n terms.

of finite N_{\max} , we test two cases: (1) the values of the final three Z_n ($n = N_{\max} - 2, N_{\max} - 1, N_{\max}$) are increased by 15% and (2) the final two Z_n ($n = N_{\max} - 1, N_{\max}$) are set to zero. As an example, we plot the number susceptibility λ_2/N_{\max} in Fig.2 as a function of μ/T at $\sqrt{s} = 27$ GeV for these two cases together with the one constructed from the full Z_n .

Let us suppose that, as μ is increased, we encounter a phase transition or a cross-over transition, and cross it. In this case, we would expect the structure of the moments to be rough in this area. At the peak position of the lower curve indicated by an arrow in Fig.2, the center line continues to increase. We write this value as $\bar{\mu}(T)$, and any transition may occur for $\mu \geq \bar{\mu}$. In other words, this position $\bar{\mu}$ is a candidate for the lower bound of the real susceptibility peak. We then check the behavior of λ_3/λ_2 and λ_4/λ_2 ; Although higher moments have large effects because of the finite N_{\max} , they may work as a good tool to detect the transition region of

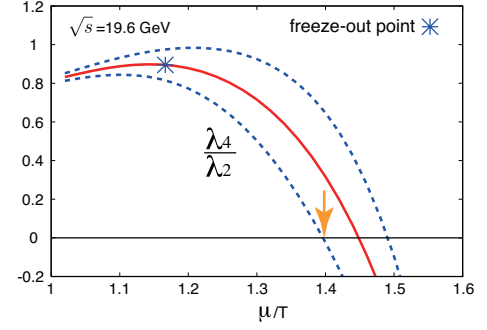


FIG. 3: Ration of the moments λ_4/λ_2 as a function of μ/T at $\sqrt{s} = 19.6$ GeV. The upper and lower curves are constructed by the same procedure as in Fig.2

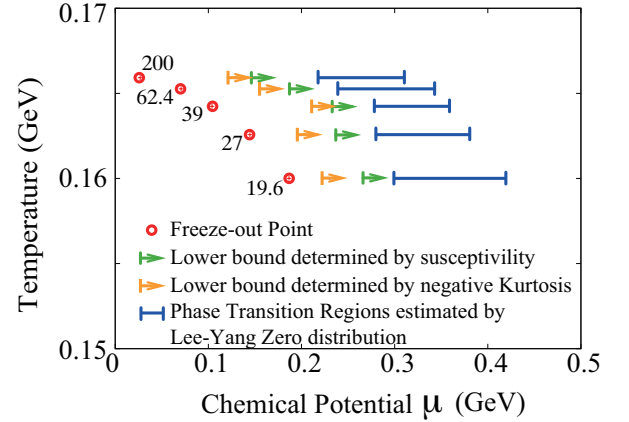


FIG. 4: Potential regions of hidden phase transition. The regions are estimated as complement of the areas where no transition is evident.

the QCD phase diagram [14]. The former ratio indicates no significant structure for $\mu \leq \bar{\mu}$. Around the freeze-out points, $\lambda_4/\lambda_2 \sim 1$ (Poisson) and it decreases to the negative values as μ increases. See Fig.3. In Refs.[15–17], it is argued that the negative value of λ_4/λ_2 is a signal of reaching the phase transition. We take the points where the lower curve of λ_4/λ_2 becomes negative (indicated by an arrow in Fig.3) as another candidate of the lower bound $\bar{\mu}(T)$ and show them in Fig.4.

Next we extend the fugacity ξ to complex values. Lee–Yang zeros (LYZs) α_l are zeros of the grand partition function $Z(\xi)$ in the complex fugacity plane; that is, $Z(\xi) = \prod_l (\xi - \alpha_l)$. The distribution of these zeros reflects the phase structure of the corresponding statistical system. Lee and Yang argued that for a finite system, no zeros appear on the real axis. In the thermodynamic limit, the number of zeros becomes infinite and the zeros coalesce onto one-dimensional curves[18]. For the first-order (second-order) phase transition, the coalescing zeros cross (pinch) the real positive ξ axis[19], whereas for the cross-over, they do not reach to the real axis.

Therefore it is important to reliably determine the

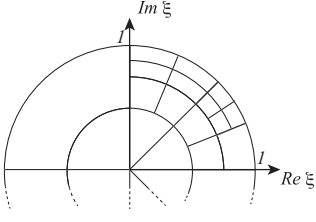


FIG. 5: Schematic of cBK contours in the divide-and-conquer search for residues.

LYZs; that is, all zeros must be found without ambiguity, and their positions in the complex fugacity plane must be determined with high accuracy. We obtain the LYZs as follows: We first map the problem to a calculation of the residue of Z'/Z :

$$Z'/Z = \sum 1/(\xi - \alpha_l). \quad (4)$$

In Eq.(4), the left hand side is integrated along a contour, and the residues inside the contour are summed according to Cauchy's theorem. Because of the symmetry $+\mu \leftrightarrow -\mu$, if α_l is a solution, i.e., $Z(\alpha_l) = 0$, then $1/\alpha_l$ is also a solution. Therefore we only need to search for residues inside the unit circle.

Fig.5 shows cut Baum-Kuchen (cBK) shape contours used in the study. Starting from $0 \leq \theta < 2\pi$, and $0 < r \leq 1$ in polar coordinates, the region is divided into four pieces, and the Cauchy integral is evaluated over each section. This divide-and-conquer process is iterated up to as many times as needed (here 20 times). When no residue is found in a section, no further divisions are applied to that section. At each divide-and-conquer level, we check the conservation of the residue sum. The technical details of this approach will be presented elsewhere.

All calculations were performed using the multiple-precision package, Fmlib[20], and the number of significant digits was 50 - 100. We checked that residues involved in the analyses presented herein are $1 + \epsilon$ with $|\epsilon| < 10^{-3}$.

With this algorithm, we can construct LYZ diagrams from Z_n . First, we study the LYZs of the lattice QCD simulation. Here we do not distinguish u and d quarks. Details of calculating Z_n with a lattice QCD simulation are given in [21], where the fugacity expansion formula [22] plays an essential role to obtain Z_n . We update 11000 trajectories including 3000 thermalization ones. The measurement is performed at each 10 (20) trajectories for $8^3 \times 4$ ($10^3 \times 4$). The Monte Carlo update is performed with the fermion measure at $\mu = 0$; thus we avoid any sign problem due to the complex fermion determinant. However, an overlap problem still exists, especially at low temperatures. When evaluating Z_n , the corresponding operators fluctuate rapidly.

The LYZ diagrams of the lattice QCD above and just below the phase-transition temperature are shown in Figs.6 and 7, respectively. For Z_n , we use data of

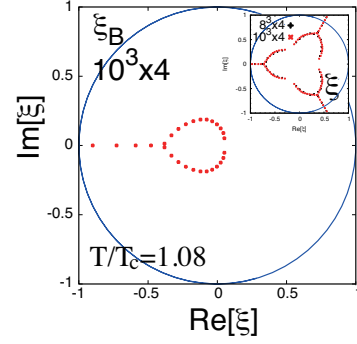


FIG. 6: LYZ diagram at $T/T_c = 1.08$ ($\beta = 1.9$) on the lattice. Lattice size is $10^3 \times 4$ and $8^3 \times 4$ and $N_{\text{Max}} = 28$ and 14, respectively.

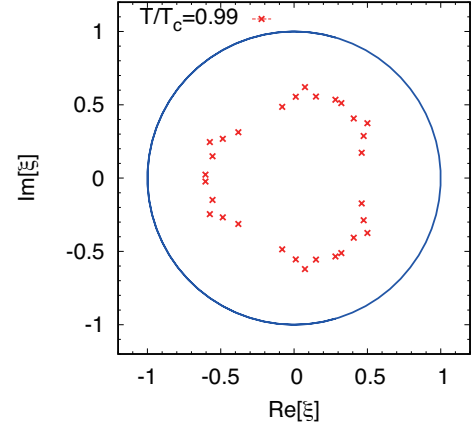


FIG. 7: LYZ diagram at $T/T_c \simeq 1.0$ ($\beta = 1.85$) on the QCD lattice. Lattice size is $8^3 \times 4$.

(Signal/Noise) ≥ 2 . Since the simulation poorly performs at lower temperatures, fewer Z_n points are available in those regions. The condition $Z_n = 0$ for $n = 1, 2 \pmod{3}$ (which can be easily proven) is imposed on the lattice data for Z_n , which guarantees $2\pi/3$ translational invariance for $\text{Im}(\mu)/T$. We evaluate the LYZs for $Z(\xi_B) = \sum_m Z_{3m} \xi_B^m$, and map the result onto $\xi = \xi_B^{1/3}$.

Note that, because the Z_n obtained in the confinement region suffer from significant noise, the LYZ diagram should be considered qualitative. However, despite this, distinctive differences between Figs.6 and 7 are apparent. At $T \sim 1.2T_c$, a line of zero accumulation appears at $\arg(\xi) = \pm\pi/3$, which indicates a Roberge-Weiss (RW) phase transition.

Roberge and Weiss discuss the regions of pure imaginary chemical potential, and find that at $\text{Im}(\mu)/T = \pi/3 + 2k\pi/3$ ($k = 0, 1$), a phase transition occurs for $T \geq T_{\text{RW}}$ [23]. By using the same lattice setup as that used in the present study, the quantity T_{RW} was estimated to be around $1.1T_c$ [24]. This phase transition exerts a clear effect on the LYZ diagram in Fig.6 where the temperature $T \sim 1.2T_c$. However, no such effect ap-

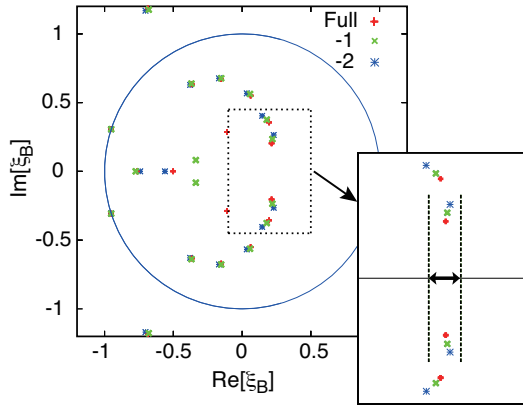


FIG. 8: LYZ diagram (STAR at $\sqrt{s} = 200$ GeV). “Full” result is calculated by using all Z_n . “-1” is by dropping a pair of Z_n of $n = \pm N_{\max}$. For “-2”, we drop further two pair Z_n . The inset is an enlarged view of the zeros near positive real axis, which gives a predicted region of QCD phase transition shown in Fig.4

pears in Fig.7, where the temperature is close to T_c .

We next consider the LYZ diagrams on the basis of RHIC Star data. We construct the grand partition function Eq.(1) for RHIC energies, $\sqrt{s} = 19.6, 27, 39, 62.4$ and 200 GeV, from the data of $P_n \geq 2$, and use the cBK method to calculate the LYZ diagrams. The result for $\sqrt{s} = 200$ GeV is shown in Fig.8. To make the finite N_{\max} effect apparent, we also calculate the LYZs by neglecting Z_n for $n = \pm N_{\max}$ (“-1”) and by neglecting Z_n for $n = \pm N_{\max}$ and $\pm(N_{\max} - 1)$ (“-2”).

Although some zeros exist on the negative real axis, these do not form a line that clearly characterizes the RW transition, which suggests that the data correspond to temperatures below T_{RW} . Remember that the net-proton number is not an exactly conserved quantity, but

it nevertheless may carry information at the time when it was born at higher temperature. Therefore, these points may be a trail of the line corresponding to the RW transition.

In the LYZ diagrams for RHIC, no zeros appear in the positive real- ξ region. Possible explanations for this result are that (i) there is no phase transition, but the cross-over occurs at these temperatures, (ii) the systems are finite, and/or (iii) the N_{\max} values are too small. The size of the fire ball produced is comparable to the QCD scale, and thus, explanation (ii) is at least partially correct. To further explore the QCD phase transition, larger N_{\max} must be attained.

Finally, we estimate where the Lee–Yang zeros would intercept or reach near to the positive real axis as the volume increases. These zones are indicated by double-headed arrows in the inset of Fig.8. In Fig.4, the corresponding regions are indicated by horizontal lines. If the multiplicities P_n with larger n were to be measured in future experiments, the QCD phase transition could be pinpointed with more precision. The further study of the relation between baryon and proton number distribution will improve the analysis here[25].

This work grew out of the stimulus provided to one of the authors (A.N.) at Workshop ‘QCD Structure’ at Wuhan by L. McLerran and N. Xu.. In addition, we would like to thank N. Xu, X. Luo, C. Sasaki, K. Shigaki and V. Skokov for valuable information. We are indebted Ph. de Forcrand and K. Morita for critical reading of the manuscript and valuable comments. A.N. wishes also to thank T. Hatsuda and M. Yahiro for continuous interests and encouragement. The calculations were done SX-9 and saho, at RCNP Osaka, RICCA at Riken and SR16000 at KEK. This work was supported by Grants-in-Aid for Scientific Research 20105003-A02-0001, 23654092 and 24340054.

-
- [1] K. Fukushima and T. Hatsuda, Rept. Prog. Phys. **74**:014001, 2011.
 - [2] M. Gyulassy and L. McLerran, Nucl. Phys. A750: 30, 2005.
 - [3] STAR Collaboration (J. Adams et al.) Nucl.Phys.A757, 102, 2005
 - [4] PHENIX Collaboration (K. Adcox et al.) Nucl.Phys. A757 (2005) 184.
 - [5] K. Fukushima, arXiv:1108.2939.
 - [6] Z. Fodor and S.D. Katz ACTA PHYSICA POLONICA B, 42 (2011), 2791.
 - [7] Ph. de Forcrand PoS (LAT2009)010, 2009.
 - [8] A. Nakamura, Phys. Lett. 149B (1984) 391.
 - [9] M.M. Aggarwal et al., Phys. Rev. Lett. **105** 022302 (2010).
 - [10] X. Luo, Quark Matter 2012 arXiv:1210.5573, to appear in Quark Matter 2012 Proceedings.
 - [11] M. A. Stephanov, K. Rajagopal, and E. V. Shuryak. Phys. Rev. Lett. **81**, 4816 (1998).
 - [12] K. Morita et al., arXiv:1211.4703 [hep-ph].
 - [13] J. Cleymans et al., Phys. Rev. C73, 034905 (2006)
 - [14] B. Friman et al., Euro. Phys. J C(2011) 71: 1694.
 - [15] R. V. Gavai and S. Gupta, Phys. Lett. B696 459, 2011.
 - [16] V. Skokov, B. Friman and K. Redlich, Phys. Rev. C83, 054904, 2011.
 - [17] M. A. Stephanov, Phys. Rev. Lett. **107**, 052301 (2011).
 - [18] C. N. Yang and T. D. Lee, Phys. Rev. **87**, 404 (1952), T. D. Lee and C. N. Yang, Phys. Rev. **87** 410(1952).
 - [19] M. A. Stephanov, Phys. Rev. D73, 094508 (2006).
 - [20] D. M. Smith, <http://myweb.lmu.edu/dmsmith/FMLIB.html>
 - [21] K. Nagata et al., Prog. Theor. Exp. Phys. 2012: 1A103.
 - [22] K. Nagata and A. Nakamura, Phys. Rev. D82 094027.
 - [23] A. Roberge and N. Weiss, Nucl. Phys. B275(1986) 734.
 - [24] K. Nagata and A. Nakamura, Phys. Rev. D83 114507.
 - [25] M. Kitazawa and M. Asakawa, Phys. Rev. C85, 021901(R) (2012).